radiation damage

Dose dependence of radiation damage for protein crystals studied at various X-ray energies

Nobutaka Shimizu,[a] Kunio Hirata,[b] Kazuya Hasegawa,[a] Go Ueno[b] and Masaki Yamamoto[a,b]*

[a]Structural Biology Group, Research and Utilization Division, Japan Synchrotron Radiation Research Institute, 1-1-1 Kouto, Sayo, Sayo-gun, Hyogo 679-5198, Japan, and [b]Division of Synchrotron Radiation Instrumentation, RIKEN SPring-8 Center, Hyogo, Japan.
E-mail: yamamoto@postman.riken.go.jp

Radiation damage to protein crystals is the most serious problem in obtaining accurate structures from protein crystallography. In order to examine the photon energy dependence of radiation damage, 12 to 15 data sets from each of nine tetragonal lysozyme crystals were collected at nine different X-ray energies (6.5, 7.1, 8.3, 9.9, 12.4, 16.5, 20.0, 24.8 and 33.0 keV) using beamline BL41XU at SPring-8. All results were compared on the basis of absorbed dose, expressed in Gray (Gy). Crystallographic statistics, such as the values of lattice constants, R_{merge} and $I/\sigma(I)$, for each data set degraded at all nine energies as the exposure time for each crystal increased. In all data sets, radiation damage was observed after the absorbed dose exceeded 10^6 Gy. However, from the point of view of crystallographic statistics normalized to the absorbed dose, no clear dependence on photon energy was observed in these results. Structural refinement showed that the average B-factor for the last data set was larger than that for the first data set at all energies tested. However, no energy dependence of radiation damage on B-factor was found. Furthermore, disruption of disulfide bonds due to radiation damage was observed in electron density maps even at the highest photon energy (33 keV) used in this study. Therefore, these results suggest that radiation damage in the energy range investigated could be evaluated based on absorbed dose without energy dependence, and that it is important to minimize the absorbed dose in a crystal sample for obtaining an accurate protein structure.

Keywords: radiation damage; X-ray energy; dose dependence.

1. Introduction

High-brilliance X-ray beams from synchrotron radiation are one of the most powerful tools for modern protein crystallography. However, this technology often results in serious problems due to radiation damage. Although the mechanism of radiation damage in cryo-cooled protein crystals has not been characterized in detail, its effect is considered to be due to several interactions. When a protein crystal absorbs X-ray photons, direct interactions occur first, causing temperature increases and dissociation of the covalent bonds. As a result of these interactions, reactive electrons, in other words free radicals, are produced (O'Neill et al., 2002). These radicals excite other covalent bonds and water molecules. This excitation propagates in the crystal, finally disrupting not only covalent bonds but also intermolecular networks forming crystal lattices. As these events are caused by absorbed photons in the crystal, it is important to consider the number of photons and their energy when discussing radiation damage.

The cryo-crystallographic method is almost always utilized for diffraction experiments at the synchrotron beamline in order to reduce radiation damage (Garman & Schneider, 1997). This is effective in significantly reducing radiation damage at beamlines where the photon flux density is around 10^{12} photons s^{-1} mm^{-2}, such as bending-magnet beamlines at SPring-8, and the damage occurs gradually during one data collection. However, at beamlines equipped with an insertion device as the light source, where the density reaches $\sim 10^{14}$ photons s^{-1} mm^{-2}, a protein crystal would receive marked radiation damage before the collection of one data set was complete, even for measurements at 100 K (Garman & Owen, 2006). The photon flux density clearly differs between these two types of beamline. However, although the probability of an interaction between an atom and an absorbed photon in a crystal can essentially be defined by the absorption

coefficient, this coefficient changes with photon energy. For these reasons the absorbed dose is widely used as the most basic factor for evaluating radiation damage (*e.g.* Sliz *et al.*, 2003; Leiros *et al.*, 2006). The absorbed dose is calculated with knowledge of a number of parameters derived from properties not only of the incident X-ray beam but also of the crystal sample. For a cryo-crystallographic measurement, the maximum absorbed dose per unit mass for the diffraction intensity to fall by half through radiation damage has been calculated by analogy with electron microscopy observations to be 2×10^7 Gy [1 Gray (Gy) = 1 J kg^{-1}] (Henderson, 1990). The Henderson limit is a predicted value; some experimentally obtained limit values have recently been reported by Owen *et al.* (2006), which indicated that a value of 3×10^7 Gy would cause an overall intensity decrease of 30% and was appropriate; beyond this, the quality of biological information obtained from the structure was likely to be compromised.

As the X-ray exposure of a protein crystal increases, broadening of diffraction spots and decreases in diffracted intensity are often observed (Blake & Philips, 1962). Crystallographic statistics, for example R_{merge}, and scaling *B*-factor also increase with radiation damage progression. Various techniques to try to avoid this phenomenon in protein crystallography have been designed and reported. For example, use of a helium gas cryostream lowers the sample temperature to around 35 K (Nakasako *et al.*, 2001; Hanson *et al.*, 2002; Teng & Moffat, 2002).

Utilization of a high X-ray energy as an alternative possible method for reducing radiation damage has been suggested, since damage is generally thought to decrease at higher X-ray energy as the absorption is lower. Over the past few decades a considerable number of studies have been conducted on the effect of photon energy on protein crystallography (Arndt, 1984; Gonzalez *et al.*, 1994; Polikarpov, 1997; Polikarpov *et al.*, 1997; Teplyakov *et al.*, 1998; Mueller-Dieckmann *et al.*, 2004, 2005; Djinović Carugo *et al.*, 2005; Weiss *et al.*, 2005). Some theoretical considerations on the effects of X-ray energy on diffraction intensity have been reported (Arndt, 1984; Polikarpov, 1997). Polikarpov *et al.* (1997) also postulated that an X-ray wavelength of 0.9 Å ($\sim$13.8 keV) is short enough to suppress radiation damage in a protein crystal. However, following an experimental investigation, Weiss *et al.* (2005) found that there was no dependence on X-ray wavelength for radiation damage between 1.0 Å ($\sim$12.4 keV) and 2.0 Å ($\sim$6.2 keV). For the elucidation of dependence of radiation damage on photon energy it is important to experimentally examine the effects over a wide energy range. In the case of organic light-atom crystals, Müller *et al.* (2002) reported that radiation damage is reduced at around 0.6 Å ($\sim$20.7 keV) to 1.0 Å ($\sim$12.4 keV) on the basis of investigation using several energies between 0.45 Å ($\sim$27.6 keV) and 1.5 Å ($\sim$8.3 keV). In the study reported here, 12 to 15 data sets from the same lysozyme crystal per energy were collected sequentially, utilizing nine different X-ray energies (6.5, 7.1, 8.3, 9.9, 12.4, 16.5, 20.0, 24.8 and 33.0 keV). The effects of radiation damage were observed at all nine energies when the absorbed dose reached more than 10^6 Gy. However, no clear energy depen-

dence was observed in the statistical parameters. Therefore, the effect of the damage appears to depend on the absorbed dose at all X-ray energies. Consistently, disruption of disulfide bonds was observed even at the highest energy (33.0 keV) used in this study. These findings are discussed in terms of the dependence of radiation damage on photon energy and absorbed dose.

2. Materials and methods

2.1. Sample preparation

Hen egg-white lysozyme crystals in the tetragonal form ($P4_32_12$) were used as the sample for this study. Crystallization was performed by hanging-drop vapor diffusion at 293 K, pH 4.2 with 100 m*M* acetate buffer including 1.25 *M* NaCl. Crystals of approximate size 100 µm $\times$ 150 µm $\times$ 150 µm were selected for diffraction measurement. Paratone-N (Hampton Research) was selected as the cryoprotectant for measurements made in a 100 K nitrogen gas stream.

2.2. Beamline conditions

Diffraction experiments were performed at beamline BL41XU of SPring-8. At BL41XU an in-vacuum undulator (Kitamura, 2000) is installed as the light source, with a magnetic periodicity of 3.2 cm and a total length of 4.5 m. The magnetic gap can be adjusted from 9.6 to 50 mm. Energy ranges emitted by this undulator are from 6.3 to 18 keV for the first harmonic and from 19 to 54 keV for the third harmonic. The beam generated is monochromated using a rotated-inclined double-crystal monochromator, with a pair of Si(111) crystals. The first crystal has a pin-post structure for direct water cooling (Yamazaki *et al.*, 1999) and the second is indirectly cooled by water. The monochromator provides X-rays of high brilliance over a wide energy range from 6.5 to 17.5 keV for the first harmonic and from 19 to 37.5 keV for the third harmonic. As the beamline 33 cm-long rhodium-coated bent mirror for vertical focusing is currently not in use, the beam is focused only in the horizontal direction by the 70 cm-long rhodium-coated bent mirror. When the energy range of the first harmonic is used, the glancing angle of this mirror is set to 3.5 mrad to eliminate higher harmonics. For utilization of X-rays from the third harmonic, the angle is altered to 1.5 mrad. The focused beam size with no cut-off at the sample position is $\sim$130 µm (horizontal) $\times$ $\sim$280 µm (vertical) (FWHM). The focused beam is shaped by two sets of quadrant slits installed on the diffractometer (see below). Energy calibration of the beamline has been performed by measuring the absorption edges of the metals, Ni *K* (8.3328 keV), Au L_{III} (11.9787 keV), Br *K* (13.4737 keV), Mo *K* (19.9995 keV) and Ag *K* (25.5140 keV). The X-ray intensity at the sample position on BL41XU is highly stable. Changes in intensity for a beam size of 100 µm $\times$ 100 µm are less than 2% over 8 h (data not shown). Since all measurements at one energy were completed within 5 h, the effect of the intensity change is negligible.

radiation damage

Table 1
Experimental conditions for each photon energy.

X-ray energy (keV)	Detector distance (mm)	Exposure time per image (s)	Irradiated time per data set (s)	Number of data sets	Photon flux (photons s^{-1})	Dose per data set (Gy)
33.0	450	5.0	900	13	1.6×10^{11}	8.2×10^{5}
24.8	310	5.0	900	12	1.6×10^{11}	1.5×10^{6}
20.0	270	1.0	180	15	3.6×10^{11}	1.1×10^{6}
16.5	180	0.3	54	15	4.0×10^{11}	5.7×10^{5}
12.4	155	0.3	54	15	5.0×10^{11}	1.3×10^{6}
9.9	155	0.5	90	15	1.3×10^{11}	9.1×10^{5}
8.3	155	1.0	180	15	8.8×10^{10}	1.7×10^{6}
7.1	155	1.5	270	15	5.5×10^{10}	2.2×10^{6}
6.5	155	1.6	288	15	5.0×10^{10}	2.5×10^{6}
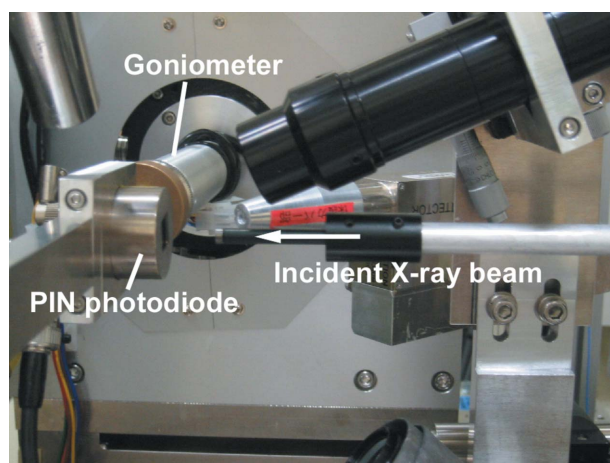
Figure 1
Experimental arrangement for measuring the photocurrent at the sample position.

2.3. Photon flux and dose calculation

In order to compare the effect of radiation damage on the basis of absorbed dose, the dose value for each data set was estimated using the program *RADDOSE* (Murray *et al.*, 2004). The incident photon flux necessary for estimating the absorbed dose was calculated from the photocurrent value measured directly with a PIN photodiode (S3590-09, HAMAMATSU Photonics) installed at the sample position (Fig. 1). The beam size at the sample position was measured by scanning with a 30 µm pinhole across the beam. Two sets of beam shaper slits were adjusted so that the beam size at the sample position would be 100 µm × 100 µm (FWHM). Fig. 2 shows the incident photon flux at the sample position as a function of X-ray energy for this beam size.

2.4. Experimental and analysis conditions

Table 1 shows the experimental conditions for the nine different photon energies. One data set comprises 180 images each with an oscillation angle of 1.0°. The detector was a Quantum 315 (Area Detector Systems Corporation) which is restricted to a minimum distance of 155 mm from the sample on beamline BL41XU. The exposure time was modified in the range from 0.3 to 5 s depending on the observed diffraction intensity. All 130 data sets were processed and scaled using

the processing results for the first and last data sets at each energy are listed in Table 2. Average *B*-factors and scale factors were derived from the Wilson plot estimated using *Truncate* (French & Wilson, 1978). Using the first data set collected at 12.4 keV, which had the best quality of all data sets, a standard structure model was first developed. After a molecular replacement procedure using coordinates of the protein atoms included in Protein Data Bank deposition 2BLX (Nanao *et al.*, 2005) up to 4 Å resolution, atomic positional and *B*-factor refinements were performed up to the maximum resolution (1.33 Å). Molecular replacement and structural refinement were carried out using *AMoRe* (Navaza, 1994) and *REFMAC5* (Murshudov *et al.*, 1997), respectively. Subsequently, 214 water molecules were automatically added to the model structure with the arp_waters feature (Lamzin & Wilson, 1993) from *REFMAC5* in CCP4i. After additional positional/*B*-factor refinements using *REFMAC5*, the standard model structure was obtained.

This model was used to evaluate other data sets with different energies or exposure times. Utilizing the protein atoms of the standard structure model, rigid-body refinement was performed to 4 Å resolution. Water molecules were excluded from the standard model and, after positional/*B*-factor refinements to 2.33 Å, these water molecules were simply merged into the protein coordinates. The final structure for each energy was acquired after additional positional/*B*-factor refinements using *REFMAC5*. The maximum resolution of all data sets was cut off at 2.33 Å at the refinement stage, which is the resolution limit of the worst diffracting data set collected at 6.5 keV. The refinement statistics for the first and last data sets are listed in Table 3 for four of the photon energies measured.
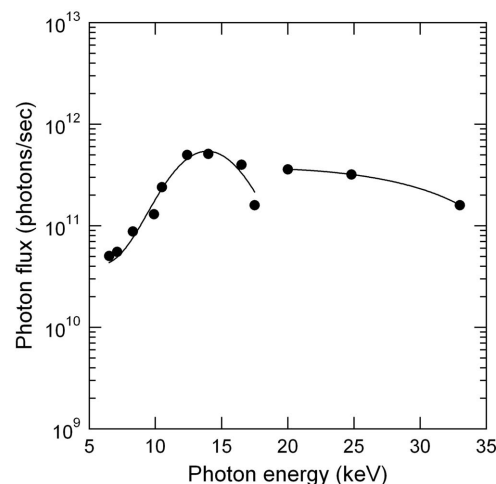
Figure 2
Photon flux at the sample position with a beam size of 100 µm × 100 µm (FWHM) as a function of photon energy.

Table 2
Results of the first and the last data sets.

Values in parentheses are for the highest-resolution shell.

X-ray energy (keV)	Resolution range (Å)	Data set number	a = b (Å)	c (Å)	R_{merge}	$\langle I/\sigma I \rangle$	Completeness (%)	Redundancy	Mosaicity (°)	Average B-factor in Wilson plot (Å²)	Scale factor
33.0	25.0–1.35	1	78.56	37.21	0.081 (0.295)	31.7 (11.5)	100.0 (100.0)	14.3 (12.9)	0.120	10.9	686.3
		13	78.59	37.24	0.081 (0.357)	28.4 (7.0)	100.0 (100.0)	13.9 (10.4)	0.148	12.1	648.0
24.8	25.0–1.21	1	78.50	37.25	0.072 (0.294)	35.7 (6.0)	98.2 (85.0)	12.6 (5.4)	0.143	8.8	475.9
		12	78.58	37.30	0.072 (0.474)	31.8 (1.8)	88.5 (34.6)	11.6 (1.9)	0.196	10.3	536.1
20.0	25.0–1.24	1	78.59	37.26	0.061 (0.294)	44.6 (6.9)	99.9 (99.4)	13.3 (7.7)	0.178	9.6	418.2
		15	78.63	37.27	0.062 (0.339)	39.1 (2.7)	96.4 (71.4)	12.9 (2.8)	0.203	10.8	485.7
16.5	25.0–1.25	1	78.55	37.24	0.064 (0.295)	36.6 (6.0)	99.5 (95.5)	12.4 (5.3)	0.117	10.0	448.4
		15	78.58	37.27	0.063 (0.305)	36.2 (3.3)	95.8 (66.0)	11.6 (2.7)	0.138	10.9	498.4
12.4	25.0–1.33	1	78.61	37.20	0.048 (0.310)	50.3 (7.0)	99.8 (98.4)	13.2 (10.1)	0.196	12.7	146.4
		15	78.66	37.21	0.049 (0.526)	46.0 (1.6)	87.2 (18.2)	12.0 (2.5)	0.297	15.9	176.4
9.9	35.0–1.50	1	78.58	37.25	0.063 (0.228)	43.2 (6.9)	99.5 (95.8)	12.5 (6.1)	0.160	14.8	93.1
		15	78.64	37.31	0.066 (0.277)	36.4 (2.8)	96.1 (63.5)	12.1 (2.9)	0.201	18.6	106.8
8.3	50.0–1.85	1	78.64	37.25	0.068 (0.162)	41.9 (13.3)	99.4 (95.9)	13.1 (13.0)	0.181	17.4	129.8
		15	78.75	37.27	0.078 (0.276)	34.3 (4.2)	99.4 (94.8)	13.2 (12.5)	0.289	24.8	178.8
7.1	50.0–2.06	1	78.46	37.29	0.067 (0.106)	40.0 (15.7)	99.0 (92.0)	12.2 (6.4)	0.150	18.0	96.2
		15	78.56	37.39	0.078 (0.257)	33.4 (6.1)	99.0 (92.0)	11.7 (6.1)	0.290	30.2	112.0
6.5	50.0–2.33	1	78.70	37.18	0.063 (0.120)	44.5 (16.9)	98.9 (90.4)	12.3 (7.8)	0.207	29.5	70.5
		15	78.77	37.22	0.073 (0.226)	37.4 (8.4)	98.9 (90.4)	12.1 (7.2)	0.350	41.7	71.2

Table 3
Typical statistics for structural refinement against the first and last data sets.

Energy (keV)	Data set number	Number of reflections	R-factor	R_{free}	Average B-factor of all atoms (Å²)
33.0	1	5315	0.162	0.254	31.69
	13	5321	0.162	0.258	32.61
24.8	1	5311	0.169	0.251	30.19
	12	5330	0.169	0.256	31.38
12.4	1	5322	0.162	0.253	33.00
	15	5325	0.163	0.263	36.10
8.3	1	5329	0.162	0.254	32.32
	15	5339	0.162	0.268	37.96

3. Results and discussion

In order to compare the dependence of radiation damage on X-ray energy in a protein crystal, it was necessary to conduct diffraction data collection over a wide range of X-ray energies. High-flux X-rays that can cause radiation damage in a relatively short time are suitable for carrying out repetitive measurement. As the light source of BL41XU at SPring-8 is an in-vacuum undulator, high flux and a wide X-ray energy range (6.5–37.5 keV) are both available. Therefore, BL41XU is considered to be a suitable beamline for performing such comparisons of energy dependence.

3.1. Processing results

Table 1 shows the experimental conditions at each X-ray energy. The detector distances were chosen based on the maximum resolution of diffraction patterns. However, the diffraction intensities at wide angles cannot be recorded at energies lower than 9.9 keV owing to the limitation on the minimum detector distance (155 mm). Exposure times at 33.0

and 24.8 keV were longer than at the other energies so as to obtain data with enough statistical accuracy, necessary owing to the phosphor efficiency of the CCD detector being optimized for 12.4 keV (∼1 Å) photons. Using different exposure times for the various energies caused no difficulties with the methodology of the experiment, since these studies were carried out on the basis of absorbed dose calculated using *RADDOSE*, which takes into account the exposure time.

Table 2 shows the processing results of the first and the last data sets at the nine energies investigated. Lattice constants of the first data sets are similar at all energies. For data sets measured at 12.4 keV and higher photon energies, resolution limits were chosen so that the values of R_{merge} in the highest-resolution shell would not exceed 30%. Resolution limits for the 9.9 keV data sets and lower photon energies were determined by the detector edge because of the limitation on the closest detector distance. In both cases the resolution limit for each data set at the same X-ray energy was fixed on that for the first set to enable quantitative comparison of statistics. Almost all of these parameters deteriorated at all energies when the first and the last data set were compared. Considerable changes were observed for R_{merge} and $\langle I/\sigma I \rangle$ in the highest-resolution shell, indicating, as expected, that crystalline deterioration owing to radiation damage influences crystallographic statistics, especially at higher resolutions. Values of completeness at 24.8 and 12.8 keV, for which the change in R_{merge} and $\langle I/\sigma I \rangle$ is relatively large, were smaller than at other energies. Although re-processing of these outlier data sets was conducted, the reason for the smaller changes could not be determined. This behavior could be due to differences in the experimental conditions; for example, the volume of cryoprotectant around the crystal sample. Average B-factors in a Wilson plot increase during the progress of the measurement, obviously showing the effect of radiation damage. Increases of

radiation damage

Wilson scale factors were also observed at all energies except at 33.0 keV; this outlier result observed at 33.0 keV is not understood.
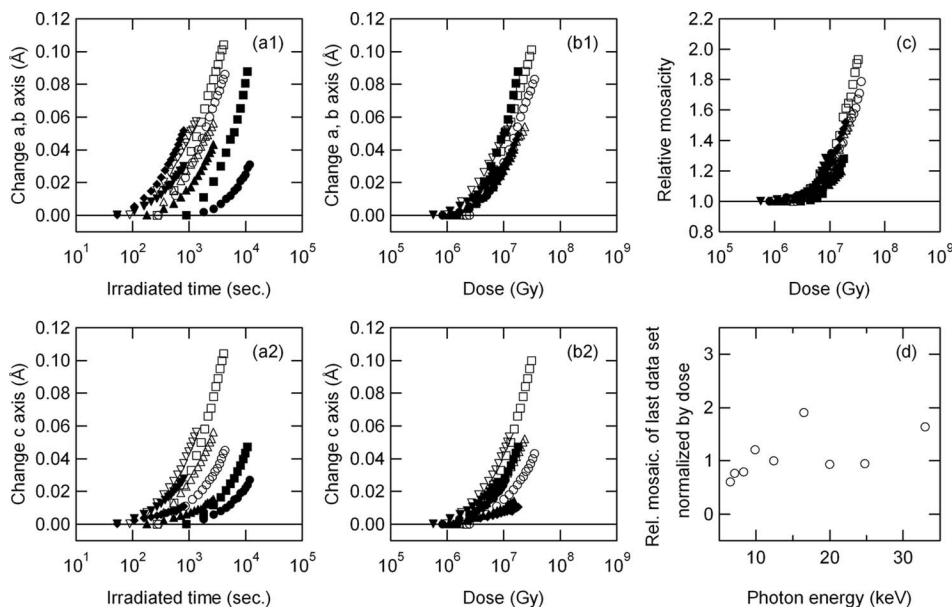
3.2. Relationship between radiation damage and dose

The effect of radiation damage on each statistical parameter obtained from the diffraction data was examined. In Fig. 3, changes in lattice constants are compared over the nine energies. The parameter 'Irradiated time' means the total exposure time per single data set, and one data point in Figs. 3(a1) and 3(a2) corresponds to one data set. Lattice constants increased along with irradiated time for all nine X-ray energies tested. Changes in lattice constants are plotted against the absorbed dose (Figs. 3b1 and 3b2). For all the data sets, radiation damage was observed after the absorbed dose exceeded 10^6 Gy. Curves plotted for all X-ray energies could almost be superimposed on one another (Figs. 3b1 and 3b2). Further comparisons were performed for changes in mosaicity values and are shown in Fig. 3(c). When plotted against absorbed dose, as for Figs. 3(b1) and 3(b2), all curves approximately overlapped. These findings indicate that the effect of radiation damage depends on absorbed dose in this X-ray energy range. However, for mosaicity values, large amounts of change were observed only at lower energies. This effect was not clearly observed in Figs. 3(b). In order to confirm whether this phenomenon was truly caused by energy dependence, values of relative mosaicity for the last data set were normalized using total absorbed dose. These normalized mosaicity values plotted against photon energy are shown in Fig. 3(d). Dependence of X-ray energy was not observed, whereas values varied from 1.9 to 0.6 between 33.0 and 6.5 keV when the value at 12.4 keV was considered to be 1.0. Thus, this result indicates that the large change in mosaicity at low energies could be explained based on increase in absorbed dose, not on energy dependence.

3.3. Structural effects of radiation damage

The interaction between absorbed photons and atoms in a crystal cause structural changes of amino acids in a protein (Burmeister, 2000; Ravelli & McSweeney, 2000; Weik et al., 2000). Disulfide bonds formed between sulfur atoms of two cysteine residues are easily influenced and disrupted by photon absorption. As the lysozyme molecule has four disulfide bonds, it is suitable for evaluating structural change caused by absorbed photons. In order to examine the effect due to radiation damage in an electron density map, structural refinements were performed against all data sets. Typical results for the structures refined against the first and last data sets are summarized in Table 3. Average B-factors for all atoms also increase as well as Wilson B-factors. Relative changes in average B-factors for all atoms at each energy are shown in Fig. 4(a). The amount of change at low X-ray energy was larger than that at high energy. This result was also observed in Fig. 3(c). However, when the values for the last data set were normalized to total absorbed dose, the change of B-factor also had no X-ray energy dependence (Fig. 4b).
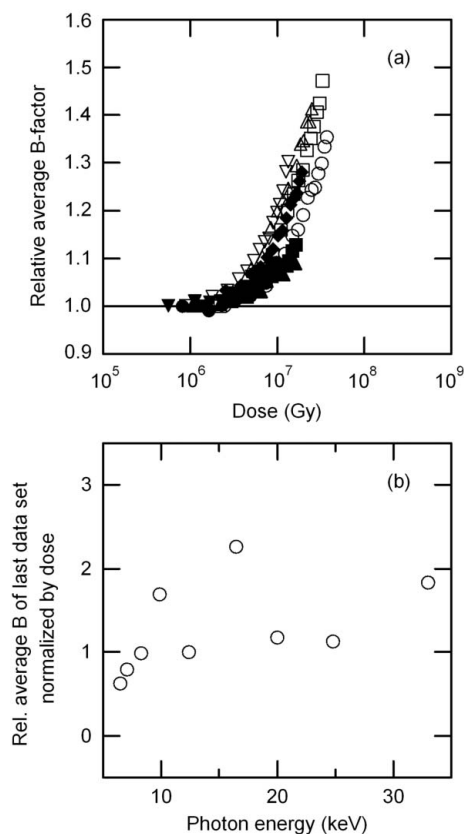
These findings indicate that for structural refinement it is important to evaluate radiation damage based on absorbed dose. The effect of radiation damage was not clearly seen in the values for crystallographic R-factor and R_{free}. Although the difference between R-factor and R_{free} became large, this might be reduced if further model buildings were performed.

Fig. 5 shows the electron density maps for the last data set at 8.3, 12.4 and 33.0 keV, obtained at 2.33 Å resolution as representative data. These maps are superimposed on two of four disulfide bonds in lysozyme, Cys76/Cys94 or Cys6/Cys127, respectively. Although the level of radiation damage is different for each bond and between energies, breakage of the disulfide bonds due to radiation damage was apparent in the electron density map even at the highest energy tested, 33.0 keV. Identical breakages were also observed not only for the other two disulfide bonds but also at all ener-
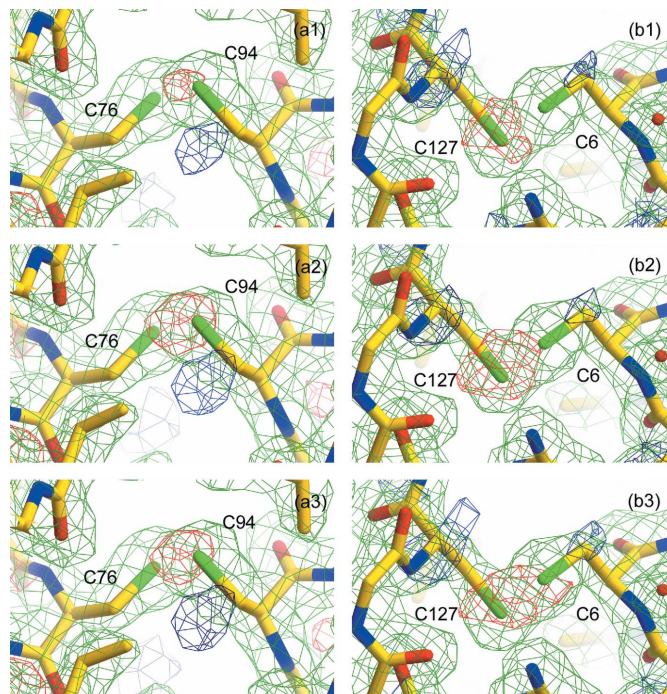

Figure 3
(a) Comparison of changes in the lattice constants, for a or b (a1) and for the c axis (a2), for nine energies. One data point represents the results from one data set. Data at 6.5, 7.1, 8.3, 9.9, 12.4, 16.5, 20.0, 24.8 and 33.0 keV are represented by the white circles, white squares, white triangles, white inverted triangles, black diamonds, black inverted triangles, black triangles, black squares and black circles, respectively. (b) For comparison, the x-axis represents absorbed dose. (c) Comparison of the change in mosaicity for the nine energies. Relative values were calculated by dividing the mosaicity of each data set by that for the first data set. (d) Comparison of the relative mosaicity normalized to total absorbed dose at each energy. These values represent relative mosaicity of the last data set after dividing by total absorbed dose at each energy; the value at 12.4 keV was designated as 1.0.

Figure 4
(*a*) Comparison of the changes in relative average *B*-factors for all atoms for the nine energies. Relative values were calculated by dividing the average *B*-factor of each data set by that of the first data set. (*b*) Comparison of the relative average *B*-factor of all atoms normalized to the total absorbed dose at each energy. These values represent relative mosaicity of the last data set after dividing by total absorbed dose at each energy; the value at 12.4 keV was designated as 1.0.

Figure 5
Electron density maps of the last data set measured at 8.3 keV (*a*1, *b*1), 12.4 keV (*a*2, *b*2) and 33.0 keV (*a*3, *b*3). Carbon, oxygen, nitrogen and sulfur atoms are colored yellow, red, blue and green, respectively. Both $2F_o - F_c$ maps contoured at 1.0σ (green) and $F_o - F_c$ maps contoured at 3.0σ (blue) or -3.0σ (red) are superimposed on two disulfide bonds formed by Cys76 and Cys94 (*a*1, *a*2, *a*3) or formed by Cys6 and Cys127 (*b*1, *b*2, *b*3), respectively. These figures were drawn using *CueMol* (http://www.cuemol.org).

gies tested (data not shown). These results indicate that utilization of high-energy X-rays could not produce data without radiation damage. Therefore, for obtaining an accurate structure, it is essential to find the best measurement conditions to minimize the absorbed dose.

4. Conclusions and future investigations

A systematic study of radiation damage to lysozyme crystals has been conducted for various X-ray energies at beamline BL41XU at SPring-8. In this study an X-ray energy dependence was clearly not observed and changes in crystallographic statistics, such as mosaicity and *B*-factor, were dependent on the absorbed dose. The possible X-ray energy dependence of radiation damage has already been investigated based on theoretical and experimental approaches (Arndt, 1984; Gonzalez *et al.*, 1994; Polikarpov, 1997; Polikarpov *et al.*, 1997; Teplyakov *et al.*, 1998; Mueller-Dieckmann *et al.*, 2005; Weiss *et al.*, 2005). In these reports, several parameters (including absorbed dose, absorption coefficient, scattering coefficient and crystal size) were considered for evaluation of energy dependence. As the absorbed dose is a physical quantity fundamentally including those parameters,

the validity of using it to estimate the radiation damage has been demonstrated in the present study. However, it is controversial to evaluate the energy dependence of the detector efficiency. Although CCD detectors are generally used at beamlines in synchrotron facilities, their efficiency at high X-ray energy, such as 33.0 keV, is not well defined. In this study the exposure time for detecting an accurate diffraction signal at higher X-ray energy was necessarily long. From the point of view of minimizing the absorbed dose, it might be difficult to directly compare two sets of high-energy data (24.8 and 33.0 keV) due to insufficient photon flux and detector sensitivity. If both the beamline optics and the detector could be optimized for high energy, energy dependence of radiation damage could be investigated in more detail.

Utilization of high energy is not an effective approach to reducing radiation damage under similar experimental environments (same kind of detector and optics) as that used at lower energy. Breakage of disulfide bonds owing to radiation damage was observed even at the highest energy tested in this study, 33.0 keV. Therefore, minimizing the absorbed dose of crystals for diffraction data collection is extremely important using any X-ray energy suitable for obtaining an accurate structure.

radiation damage

to all members of both the Structural Biology Group at JASRI/SPring-8 and the Synchrotron Radiation Instrumentation Group at RIKEN SPring-8 Center.

References

Arndt, U. W. (1984). *J. Appl. Cryst.* **17**, 118–119.
Blake, C. C. F. & Philips, D. C. (1962). *Biological Effects of Ionizing Radiation at the Molecular Level*, pp. 183–191. Vienna: International Atomic Energy Agency.
Burmeister, W. P. (2000). *Acta Cryst.* D**56**, 328–341.
Djinović Carugo, K., Helliwell, J. R., Stuhrmann, H. & Weiss, M. S. (2005). *J. Synchrotron Rad.* **12**, 410–419.
French, G. S. & Wilson, K. S. (1978). *Acta Cryst.* A**34**, 517.
Garman, E. F. & Owen, R. L. (2006). *Acta Cryst.* D**62**, 32–47.
Garman, E. F. & Schneider, T. R. (1997). *J. Appl. Cryst.* **30**, 211–237.
Gonzalez, A., Denny, R. & Nave, C. (1994). *Acta Cryst.* D**50**, 276–282.
Hanson, B. L., Harp, J. M., Kirschbaum, K., Schall, C. A., DeWitt, K., Howard, A., Pinkerton, A. A. & Bunick, G. J. (2002). *J. Synchrotron Rad.* **9**, 375–381.
Henderson, R. (1990). *Proc. R. Soc. London Ser. B*, **241**, 6–8.
Kitamura, H. (2000). *J. Synchrotron Rad.* **7**, 121–130.
Lamzin, V. S. & Wilson, K. S. (1993). *Acta Cryst.* D**49**, 129–147.
Leiros, H.-K. S., Timmins, J., Ravelli, R. B. G. & McSweeney, S. M. (2006). *Acta Cryst.* D**62**, 125–132.
Mueller-Dieckmann, C., Panjikar, S., Tucker, P. A. & Weiss, M. S. (2005). *Acta Cryst.* D**61**, 1263–1272.
Mueller-Dieckmann, C., Polentarutti, M., Djinović Carugo, K., Panjikar, S., Tucker, P. A. & Weiss, M. S. (2004). *Acta Cryst.* D**60**, 28–38.
Müller, R., Weckert, E., Zellner, J. & Drakopoulos, M. (2002). *J. Synchrotron Rad.* **9**, 368–374.
Murray, J. W., Garman, E. F. & Ravelli, R. B. G. (2004). *J. Appl. Cryst.* **37**, 513–522.
Murshudov, G. N., Vagin, A. A. & Dodson, E. J. (1997). *Acta Cryst.* D**53**, 240–255.
Nakasako, M., Sawano, M. & Kawamoto, M. (2001). *Rigaku J.* pp. 47–53.
Nanao, M. H., Sheldrick, G. M. & Ravelli, R. B. G. (2005). *Acta Cryst.* D**61**, 1227–1237.
Navaza, J. (1994). *Acta Cryst.* A**50**, 157–163.
O'Neill, P., Stevens, D. L. & Garman, E. F. (2002). *J. Synchrotron Rad.* **9**, 329–332.
Otwinowski, Z. & Minor, W. (1997). *Methods Enzymol.* **276**, 307–326.
Owen, R. L., Rudiño-Piñera, E. & Garman, E. F. (2006). *Proc. Natl. Acad. Sci. USA*, **103**, 4912–4917.
Polikarpov, I. (1997). *J. Synchrotron Rad.* **4**, 17–20.
Polikarpov, I., Teplyakov, A. & Oliva, G. (1997). *Acta Cryst.* D**53**, 734–737.
Ravelli, R. B. G. & McSweeney, S. M. (2000), *Structure*, **8**, 315–328.
Sliz, P., Harrison, S. C. & Rosenbaum, G. (2003). *Structure*, **11**, 13–19.
Teng, T.-Y. & Moffat, K. (2002). *J. Synchrotron Rad.* **9**, 198–201.
Teplyakov, A., Oliva, G. & Polikarpov, I. (1998). *Acta Cryst.* D**54**, 610–614.
Weik, M., Ravelli, R. B. G., Kryger, G., McSweeney, S. M., Raves, M. L., Harel, M., Gros, P., Silman, I., Kroon, J. & Sussman, J. L. (2000). *Proc. Natl. Acad. Sci. USA*, **97**, 623–628.
Weiss, M. S., Panjikar, S., Mueller-Dieckmann, C. & Tucker, P. A. (2005). *J. Synchrotron Rad.* **12**, 304–309.
Yamazaki, H., Kimura, H., Kagaya, I., Yamashita, C. & Ishikawa, T. (1999). *Proc. SPIE*, **3773**, 21–29.